Thermodynamic description of heat and spin transport in magnetic nanostructures

Laurent Gravier,* Santiago Serrano-Guisan, François Reuse, and Jean-Philippe Ansermet
Institut de Physique des Nanostructures, Ecole Polytechnique Fédérale de Lausanne, CH-1015 Lausanne-EPFL, Switzerland
(Received 1 July 2005; revised manuscript received 11 October 2005; published 25 January 2006)

Spin-dependent heat and charge transport perpendicular to the plane of magnetic Co/Cu multilayers was studied experimentally and interpreted in the framework of the thermodynamics of irreversible processes. The thermogalvanic voltage(TGV) is introduced. It measures the ac voltage response to a small temperature oscillation while a dc current is driven through the sample. TGV presents a magnetic response (MTGV) of 50%, much larger than magnetoresistance (GMR) and the magneto-thermoelectrical power (MTEP). The linear equations for transport of heat, charge, and spin-polarized currents in magnetic and nonmagnetic mediums are applied to a multilayer structure. The role of spin mixing in GMR, MTEP, and MTGV is shown. In particular, the asymmetry of the spin-mixing gives rise to spin-dependent effective Peltier coefficients. The three measurements can be accounted for with two parameters expressing the spin dependence of the transport coefficients.

DOI: 10.1103/PhysRevB.73.024419 PACS number(s): 75.47.−m, 72.25.−b, 72.15.Jf

I. INTRODUCTION: THE INTERFACE TRANSPORT

Ever since the study of Sir W. Thomson in 1856 on ferromagnetic thermocouples, the magneto-thermoelectric properties of ferromagnetic materials has attracted numerous experimental works.[1,2] The theoretical descriptions of heat and charge transport in magnetic medium has also drawn attention for a long time.[3–6] The discovery of the giant magnetoresistance (GMR) (Refs. 7 and 8) with the current perpendicular to the plane (CPP) (Refs. 9 and 10) brought forth the concept of spin dependent transport in layered structures.[11]

The magneto-thermoelectrical power (MTEP) of ferromagnetic layered structures has been studied. All measurements, performed with the heat current in the plane, presented a high magnetic response of the thermoelectrical power.[12] A usual analysis consists of comparing GMR and MTEP through the Mott formula, in a direct way,[13] in the framework of spin-dependent transport[14] or including all relevant spin asymmetry.[15] MTEP measurements with CPP were obtained[16] and were discussed in the same fashion.

We present in this paper heat and charge transport in magnetic nanostructures with current perpendicular to the interfaces. The significance of the data is brought out by a description of nonequilibrium thermodynamics, in the linear regime, of heat and charge transport in ferromagnets. To the author's knowledge, the use of this approach was reported only twice in the literature. Johnson and Silsbee focused on ferromagnet/nonferromagnet interface transport of a charge, heat, and magnetization currents.[17,18] Wegrowe set the kinetic equations in a metallic ferromagnet, leaving out the heat transport.[19] This approach allows us to express the mixed effects of charge and heat currents while taking into account the spin dependence of the transport coefficients.

Thus, we analyze a novel measurement which consists in monitoring the ac thermoelectric power of multilayered nanowires subjected to intense dc charge current.[20] We call the observed response the magneto-thermogalvanic voltage (MTGV). The magnetic response of this signal is much larger than the GMR or the MTEP.

Flux conservation at the interfaces between layers in a 1D model and the hypothesis of uniform gradients inside each layer complete this "three-current" model of spin-dependent heat and charge transport in ferromagnetic structures. This description includes spin mixing with a spin asymmetry. It could also take into account a spin-dependent average entropy per charge. However we find that all our data can be accounted for without introducing this term. The MTGV is shown to arise from a Peltier effect characteristic of transport perpendicular to multilayers. The three-current model demonstrate that the asymmetry in spin mixing implies spin-dependent Seebeck coefficients.

II. EXPERIMENT

A. Multilayered nanowires by template synthesis

The samples are obtained by a technique of electrodeposition in tracked-etched polymer membrane templates.[21,22] Gold layers are sputtered on both side of a porous polymers membrane. The bottom layer operates as the working electrode for electrodeposition. The pores, typically 6 μm long and with a diameter ranging from 30 to 60 nm, are filled electrochemically with a series of 300 bilayers of Co and Cu, 10 nm each.[23] The growing nanowires are electrically contacted when reaching the top gold membrane, thin enough ($\sim$50 nm) to leave the pores open (Fig. 1).The high aspect ratio of such a structure insures currents perpendicular to the layers (CPP geometry). Additionally, monitoring the potential between both Au layers allows us to limit the contact to a single nanowire.[24]

B. Transports measurements

The sample holder is installed in a cryostat that allows temperatures from 300 K down to 13 K, between the poles of a resistive magnet reaching 9 kG. The nanostructures are wired to two separate loops that can be independently connected to ac or dc instruments. The resistance is measured by conventional detection of the ac voltage due to an dc current source [Fig. 2(a)].

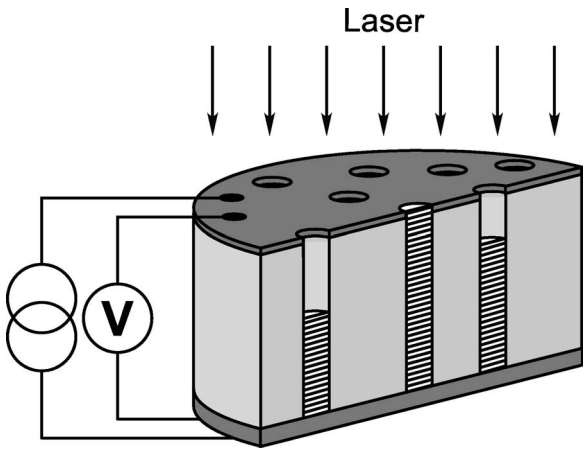

FIG. 1. Schematics of our samples. A multilayer nanowire (hatch) is embedded in a polymer membrane (light grey), and electrically contacted to gold layers (dark grey). The nanowire is heated by a laser beam from the top.

The current loop is open for the thermoelectrical power measurements (TEP) [Fig. 2(b)]. The heat source is a chopped laser beam lead by optical fiber and focused on the nanowire "top" junction by an *in situ* optical lens.[26] The optical density is about 10 W cm^{-2} for a light spot diameter below 0.5 mm. The laser spot is scanned over the surface until the signal is maximum. Lighting the top side of the membrane with a chopped light forces both temperature drop ΔT and the spatial average of the temperature of the nanowire $\bar{T}$ to oscillate at the same frequency. The ac thermoelectrical power V_{ac} is detected in phase with the oscillatory light power P_{ac} (square waveform). In our metallic wire, of a length scale of a few tens of micrometers, the temperature reaches equilibrium in less than 1 μs. Therefore we choose low enough frequencies ($<10^5$ Hz) to let the temperature gradient to be frankly established (typically 22 Hz).

The TEP protocole is extended to MTGV measurements, as sketched in Fig. 2(c). The ac voltage detection is locked to the oscillatory light power P_{ac} while a steady current I_{dc} is maintained through the wire. The temperature of the wires under currents of high density was monitored by resistance measurements.[25] The temperature rise due to the Joule heating is of no more than a few Kelvin for wires as small as 50 nm in diameter.[26]

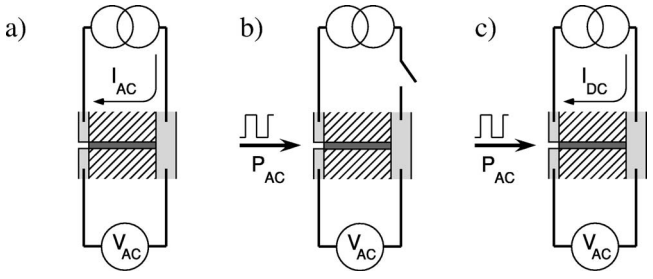

FIG. 2. Nanowire (grey) embedded in a membrane (hatched), and electrically contacted to Au layers (light grey). The three different measurement protocoles are (a) GMR, (b) MTEP, and (c) MTGV.

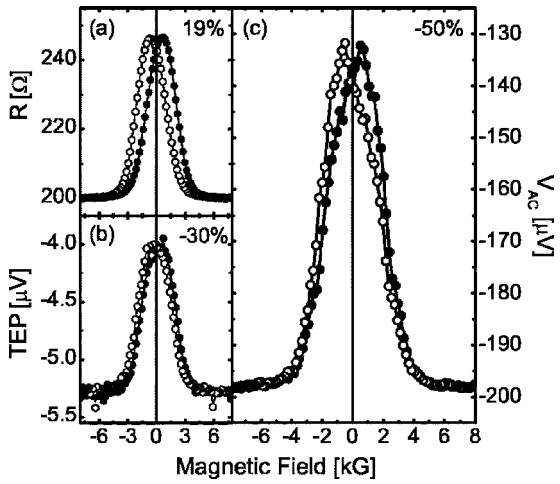

FIG. 3. (a) GMR, (b) MTEP, and (c) MTGV curves at 15 K. The MTGV data are measured under a continuous current of −200 μA. Full (open) circles indicate field sweep up (down).

C. Results

We investigated the effect of an external magnetic field $\mu_0 H$ on the transport properties of wires perpendicular to the field. We present the data of a representative sample, among the fifteen samples measured. Measurements performed at 15 K are reported in Fig. 3. The three GMR, MTEP, and MTGV curves exhibit the same bell-like shape, attributed to the progressive transition from the antiparallel (AP) to the parallel (P) magnetic configurations of the ferromagnetic layers.

The GMR ratio about 19% [Fig. 3(a)] attests to the high quality of the sample. The magnetic response of the thermoelectrical power [Fig. 3(b)] is about 30%. This MTEP ratio is thus higher than the GMR ratio. It was accounted for in terms of the spin dependence of the thermopower ε.[16,27] The MTGV is the magnetic field dependence of V_{ac} under a continuous current I_{dc} of −200 μA [Fig. 3(c)]. The MTGV ratio of about 50% is clearly higher than both GMR and MTEP ratios. Figure 4 shows that the voltage V_{ac} is practically pro-

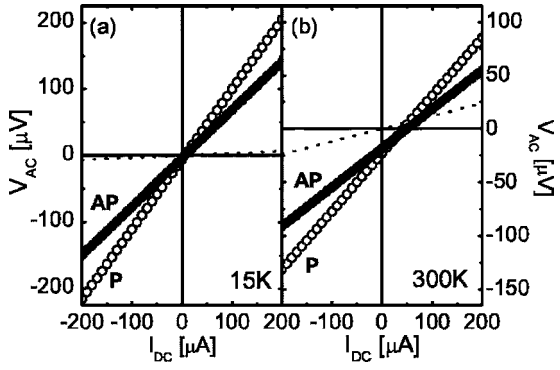

FIG. 4. V_{ac} voltage as a function of I_{dc} for zero (full circles, ●) and saturation (open circles, ○) magnetic fields at (a) 15 K and (b) 300 K. The dotted line is the expectation if only heating effects are considered.

portional to the current I_{dc}, and the slope $\partial V_{ac}/\partial I_{dc}$ strongly depends on the applied magnetic field. The change in slope is in essence what is measured in MTGV in Fig. 3. The small intercept at $I_{dc}=0$ is the MTEP. It is as small as expected for metals at low temperature.[28]

The linear dependence on the current points to a process independent of the thermopower. The enhanced magnetic response cannot strictly arise from GMR or MTEP effects. A more complex process must be invoked. Modeling with linear transport theory for heat and electrical currents clarifies what MTGV reveals, as shown below.

III. THE THREE-CURRENT MODEL

A. Constitutive equations

We apply the theory of the thermodynamics of irreversible processes in the linear approximation.[29] Electrons with different spin orientations are treated as two different charge carriers, indexed as + and −. Each type of charge carrier has its chemical potential. As in electrochemistry, the chemical potential and the electric potential add.[30] The generalized forces are the gradients of this sum of potentials and the gradient of the temperature. We assume a linear relationship between these generalized forces and their associated currents: the current $\mathbf{j}_+$ of spin +, $\mathbf{j}_-$ of spin − and $\mathbf{j}_s$ of entropy.

$$\begin{pmatrix}\mathbf{j}_s\\ \mathbf{j}_+\\ \mathbf{j}_-\end{pmatrix}=-\begin{pmatrix}L_{ss} & L_{s+} & L_{s-}\\ L_{+s} & L_{++} & L_{+-}\\ L_{-s} & L_{-+} & L_{--}\end{pmatrix}\begin{pmatrix}\boldsymbol{\nabla}T\\ \boldsymbol{\nabla}\mu_+ - q_+\mathbf{E}\\ \boldsymbol{\nabla}\mu_- - q_-\mathbf{E}\end{pmatrix}. \tag{1}$$

The number of free parameters is reduced through the Onsager reciprocal symmetry relations $[L_{ij}(H)=L_{ji}(-H),\ i\neq j]$ and also the symmetry according to which a (+) spin which is a majority spin in a field H is a minority spin in a field $-H$ and vice versa. Therefore, we have the relations $L_{+s}(H)=L_{s+}(-H)=L_{s-}(H)$ and $L_{-s}(H)=L_{s-}(-H)=L_{s+}(H)$.

We see in Eq. (1) that L_{+-} implies a contribution to the spin-up current by the down spins. This contribution is proportional to the force on the down spins. This process is characteristic of the so-called spin mixing. In such a process, spins flip while the charge carrier retains its momentum.[14] The symmetry relations keep the L_{+-} and L_{-+} parameters free of any constraints $[L_{+-}(H)=L_{-+}(-H)=L_{+-}(H)]$.

In doing so, we assume that the amplitudes of the coefficients do not depend on the magnetic field. Indeed, a field is applied, but it is used to change the relative orientation of the magnetization of the subsequent layers. In this model, the phenomena are accounted for without assuming that the intrinsic transport parameters are field dependent.

The electrochemical potential for each kind of carrier is developed as $\mu_+=\mu_0+\Delta\mu$ and $\mu_-=\mu_0-\Delta\mu$, with μ_0 the average electrochemical potential of electrons, and $\Delta\mu$ the shift induced by the polarization driven by the current. We denote $\boldsymbol{\nabla}\mu_0-q\mathbf{E}=q\boldsymbol{\nabla}V$. Therefore, with the charge of the electrons set as $q=q_+=q_-=-e$, Eq. (1) rewrites as

$$\begin{pmatrix}\mathbf{j}_s\\ \mathbf{j}_+\\ \mathbf{j}_-\end{pmatrix}=-\begin{pmatrix}L_{ss} & L_{s+}+L_{s-} & L_{s+}-L_{s-}\\ L_{s-} & L_{++}+L_{+-} & L_{++}-L_{+-}\\ L_{s+} & L_{--}+L_{-+} & -L_{--}+L_{-+}\end{pmatrix}\begin{pmatrix}\boldsymbol{\nabla}T\\ q\boldsymbol{\nabla}V\\ \boldsymbol{\nabla}\Delta\mu\end{pmatrix}. \tag{2}$$

We develop now these expressions in terms of the total charge flux $\mathbf{j}_n=\mathbf{j}_++\mathbf{j}_-$ and the spin current $\mathbf{j}_p=\mathbf{j}_+-\mathbf{j}_-$ which expresses the spin polarization of the charge flux. The flux vector is defined as $\mathbf{J}=(\mathbf{j}_s,\mathbf{j}_n,\mathbf{j}_p)$, the generalized forces are denoted by the vector $\nabla X=(\nabla T,q\nabla V,\nabla\Delta\mu)$. The linear dependence can thus be written $\mathbf{J}=\tilde{L}\cdot\boldsymbol{\nabla}X$ or

$$\begin{pmatrix}\mathbf{j}_s\\ \mathbf{j}_n\\ \mathbf{j}_p\end{pmatrix}=-\begin{pmatrix}L_{ss} & L_{s+}+L_{s-} & L_{s+}-L_{s-}\\ L_{s+}+L_{s-} & L_{++}+L_{--}+L_{+-}+L_{-+} & L_{++}-L_{--}-L_{+-}+L_{-+}\\ -L_{s+}+L_{s-} & L_{++}-L_{--}+L_{+-}-L_{-+} & L_{++}+L_{--}-L_{+-}-L_{-+}\end{pmatrix}\begin{pmatrix}\boldsymbol{\nabla}T\\ q\boldsymbol{\nabla}V\\ \boldsymbol{\nabla}\Delta\mu\end{pmatrix}. \tag{3}$$

B. Relation to usual parameters

We can now proceed to relate each L_{ij} to transport parameters. It is usual to related the kinetic coefficients to the familiar parameters σ and κ, the electric and thermal conductivities, and ε the Seebeck coefficient (or thermopower). This is possible by identifying terms of the matrix $\tilde{L}$ to the phenomenological parameters that describe conventional measurements.[29]

In the present case, we distinguish the charge conductivities σ_+ and σ_-, and the Seebeck coefficients ε_+ and ε_- of each currents. Applying successively Eq. (3) to express Ohm's Law, the heat conduction and the Seebeck voltage (Appendix A) we can establish

$$\tilde{L} = -\begin{pmatrix} \frac{\kappa}{T} + \varepsilon_+\varepsilon_-(\sigma_+ + \sigma_-) & \frac{\sigma_+\varepsilon_+ + \sigma_-\varepsilon_-}{q} & \frac{\sigma_-\varepsilon_- - \sigma_+\varepsilon_+}{q} \\ \frac{\sigma_+\varepsilon_+ + \sigma_-\varepsilon_-}{q} & \frac{\sigma_+ + \sigma_-}{q^2} + L_{+-} + L_{-+} & \frac{\sigma_+ - \sigma_-}{q^2} - L_{+-} + L_{-+} \\ \frac{\sigma_+\varepsilon_+ - \sigma_-\varepsilon_-}{q} & \frac{\sigma_+ - \sigma_-}{q^2} + L_{+-} - L_{-+} & \frac{\sigma_+ + \sigma_-}{q^2} - L_{+-} - L_{-+} \end{pmatrix}. \quad (4)$$

Electrons in ferromagnetic (F) layers are either majority ($\uparrow$) or minority ($\downarrow$), depending on the orientation of the magnetization. Accordingly, in a layer F with $\Uparrow$ magnetization, its matrix $\tilde{L}_{\Uparrow}$ is set with spin + as majority and spin − as minority, then denoted $\uparrow$ and $\downarrow$, respectively. On the contrary, for $\Downarrow$ layers the matrix $\tilde{L}_{\Downarrow}$ will be written replacing + with $\downarrow$ and − with $\uparrow$.

The charge conductivities in F layers are expressed by the relation[11]

$$\sigma_{\uparrow(\downarrow)} = \frac{\sigma_F}{2}(1 \pm \beta), \quad (5)$$

where β accounts for the spin-dependence of the carrier conductivities as

$$\beta = \frac{\sigma_\uparrow - \sigma_\downarrow}{\sigma_\uparrow + \sigma_\downarrow}. \quad (6)$$

A complete model for GMR would introduce spin-dependent interface resistance and spin relaxation in each layer. For the sake of clarity, we neglect interface resistance here. We know that our samples, this effect is not dominant.[31] The spin-diffusion length is much larger that the layer thickness[32] therefore we assume uniform gradients inside each layer. We introduced the coefficient $\Delta L_s/q = L_{s+} - L_{s-}$ that expresses the difference of entropy carried by each current. According Eq. (4), $\Delta L_s = \sigma_-\varepsilon_- - \sigma_+\varepsilon_+$. Since the Seebeck coefficient of a F layer writes as the composition of the two parallel currents + and − as $\varepsilon_F = (\sigma_+\varepsilon_+ + \sigma_-\varepsilon_-)/(\sigma_+ + \sigma_-)$,[33] we can deduce the expressions of ε_+ and ε_- as a function of ΔL_s, σ_F, ε_F and β, for both magnetization configurations, to be as follows:

$$\varepsilon^{\Uparrow}_{\uparrow(\downarrow)} = \frac{\varepsilon_F \mp \frac{\Delta L_s}{\sigma_F}}{1 \pm \beta}; \quad \varepsilon^{\Downarrow}_{\uparrow(\downarrow)} = \frac{\varepsilon_F \pm \frac{\Delta L_s}{\sigma_F}}{1 \pm \beta}. \quad (7)$$

The spin mixing terms L_{+-} and L_{-+} are kept track of through their difference $\Delta L/q^2 = L_{+-} - L_{-+}$ only. To simplify the algebra, we assume here that the conductivities due to the spin-mixing are negligible compared to the direct conductivities σ_+ and σ_-.

With the above defined parameters, the full matrix of F layers $\Uparrow$ and $\Downarrow$ becomes

$$\tilde{L}_{\Uparrow(\Downarrow)} = -\begin{pmatrix} \frac{\kappa_F}{T} + \sigma_F\varepsilon_F^2\frac{1 - \frac{\Delta L_s^2}{\sigma_F^2\varepsilon_F^2}}{1 - \beta^2} & \frac{\sigma_F\varepsilon_F}{q} & \pm\frac{\Delta L_s}{q} \\ \frac{\sigma_F\varepsilon_F}{q} & \frac{\sigma_F}{q^2} & \pm\beta\frac{\sigma_F}{q^2} \mp \frac{\Delta L}{q^2} \\ \mp\frac{\Delta L_s}{q} & \pm\beta\frac{\sigma_F}{q^2} \pm \frac{\Delta L}{q^2} & \frac{\sigma_F}{q^2} \end{pmatrix}. \quad (8)$$

In a nonmagnetic layer N, there is no discrimination between spin channels, which implies $\sigma_\uparrow = \sigma_\downarrow = \sigma_N/2$ [i.e., $\beta = 0$ in Eq. (5)], $\varepsilon_\uparrow = \varepsilon_\downarrow = \varepsilon_N$ and $\Delta L = \Delta L_s = 0$. Then

$$\tilde{L}_N = -\begin{pmatrix} \frac{\kappa_N}{T} + \sigma_N\varepsilon_N^2 & \frac{\sigma_N\varepsilon_N}{q} & 0 \\ \frac{\sigma_N\varepsilon_N}{q} & \frac{\sigma_N}{q^2} & 0 \\ 0 & 0 & \frac{\sigma_N}{q^2} \end{pmatrix}. \quad (9)$$

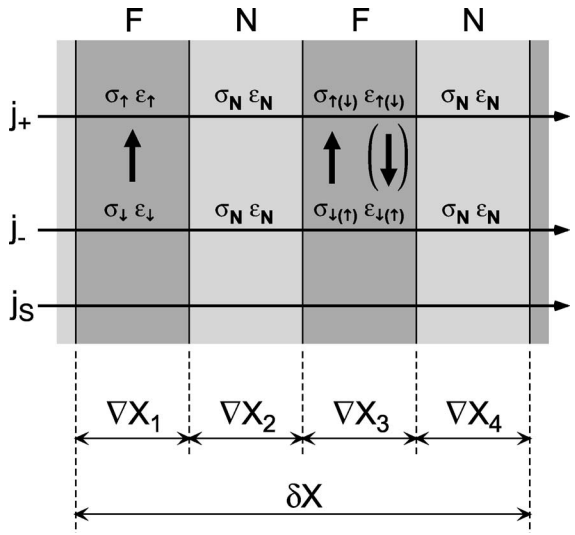

FIG. 5. Fluxes and forces over two *F-N* bilayers for both *P* and AP magnetic configurations.

C. Transport through bilayers

To probe the effect on transport of the magnetic configuration of a multilayer structure, we establish the potential difference at the ends of a system composed of two $F-N$ bilayers. The index $i=1,3$ label the ferromagnetic layers, and $i=2,4$ the nonmagnetic ones (Fig. 5).We arbitrarily set the magnetization of the first layer in the $\Uparrow$ configuration, and denote the second one with the index $m=\Uparrow,\Downarrow$ for the parallel (P) or antiparallel (AP) configurations, respectively. We assume uniform gradients, so the drop of $\mathbf{X}$ over two bilayers is given by

$$-\delta\mathbf{X} = d(\boldsymbol{\nabla}X_1 + \boldsymbol{\nabla}X_2 + \boldsymbol{\nabla}X_3 + \boldsymbol{\nabla}X_4) \tag{10}$$

with d the thickness of each layer.

The conservation of the flux vector provides the remaining equations. We emphasize here that, unlike the typical description of the Peltier effect, there is *no heat transfer* to the interface from outside. This assumption is supported by the particular 1D geometry of the metallic nanowire embedded in a polymer matrix: the heat resistance between metal and polymer is known to be quite large whereas a good heat flux is insured along the metallic wire. Furthermore, since layers are typically more than 50 nm in diameter and 5 nm in thickness, we can assume that the interfaces are infinitely extended. Therefore in this 1D approximation, forces and fluxes must develop *inside* the layers, *normal* to the interfaces.

The conservation of the fluxes at the interfaces imposes $\mathbf{J}_i=\mathbf{J}_{i+1}$ $(i=1,2,3)$,

$$\mathbf{J} = \widetilde{L}_{\Uparrow}\boldsymbol{\nabla}X_1 = \widetilde{L}_N\boldsymbol{\nabla}X_2 = \widetilde{L}_m\boldsymbol{\nabla}X_3 = \widetilde{L}_N\boldsymbol{\nabla}X_4. \tag{11}$$

Equations (10) and (11) set four equations for the four unknown gradients ∇X_i. It is a matter of straightforward arithmetics to solve for each and find

$$\mathbf{J}^{P(\mathrm{AP})} = \widetilde{Y}^{P(\mathrm{AP})}\frac{\delta\mathbf{X}}{d},$$

$$\widetilde{Y}^{P(\mathrm{AP})} = -[\widetilde{L}_{\Uparrow}^{-1} + \widetilde{L}_N^{-1} + \widetilde{L}_m^{-1} + \widetilde{L}_N^{-1}]^{-1}, \tag{12}$$

with the configurations $P(\mathrm{AP})$ for $m=\Uparrow(\Downarrow)$. In $\delta\mathbf{X}=(\delta T, -e\delta V, \delta\Delta\mu)$, the term $\delta\Delta\mu=0$ as we assume $\Delta\mu$ periodic over two bilayers. Then we can derive from Eq. (12) the potential difference through two bilayers

$$\delta V = \frac{d}{q^2 Y_{22}} j_e - \frac{Y_{21}}{qY_{22}}\delta T \tag{13}$$

with $j_e=qj_n$. This equation can be extended to the whole nanowire of length L, of cross section A and composed of n identical bilayers in series. The experiment imposes a temperature drop $\Delta T=n\delta T/2$. The condition of ΔT very small in front of the bath temperature T_b allows to assume the transport parameters to be constant along the nanowire. Then, the overall voltage drop $V=n\delta V/2$ across the whole nanowire experiencing a dc current $I=A\cdot j_e$ is found to be

$$V = \frac{L}{4A}\frac{1}{q^2 Y_{22}} I - \frac{Y_{21}}{qY_{22}}\Delta T. \tag{14}$$

This equation is used in what follows to analyze the transport measurements.

IV. EFFECTIVE TRANSPORT COEFFICIENTS

In this section, GMR is expressed in terms of the two spin current model, MTEP and MTGV in terms of one charge current and the heat current. The spin asymmetry of the Seebeck coefficients is then discussed.

A. GMR

We apply our model to the GMR. Under the condition of uniform temperature ($\Delta T=0$), Eq. (14) is reduced to its charge-current dependent term, and the GMR ratio between P and AP magnetic configurations becomes

$$\frac{R_{\mathrm{AP}} - R_P}{R_{\mathrm{AP}}} = \frac{\Delta R}{R_{\mathrm{AP}}} = 1 - \frac{Y_{22}^{\mathrm{AP}}}{Y_{22}^{P}} \tag{15}$$

with the matrixes $\widetilde{Y}^{P(\mathrm{AP})}$ derived from Eqs. (8) and (9) reduced to their bottom right submatrixes

$$L_{\Uparrow(\Downarrow)} = -\frac{\sigma_F}{e^2}\begin{pmatrix} 1 & \pm\beta \mp \dfrac{\Delta L}{\sigma_F} \\ \pm\beta \pm \dfrac{\Delta L}{\sigma_F} & 1 \end{pmatrix}, \tag{16a}$$

$$L_N = -\frac{\sigma_N}{e^2}\begin{pmatrix} 1 & 0 \\ 0 & 1 \end{pmatrix}. \tag{16b}$$

Under these conditions, the literal expression of the GMR ratio is[38]

$$\frac{\Delta R}{R_{\mathrm{AP}}} = \frac{\beta^2 - \dfrac{\Delta L^2}{\sigma_F^2}}{\left[1 + \dfrac{\sigma_F}{\sigma_N}\left(1 - \beta^2 + \dfrac{\Delta L^2}{\sigma_F^2}\right)\right]^2}. \tag{17}$$

When modeling the multilayer structures by two independent magnetic layers, i.e., without N layers (equivalently posing $\sigma_N \to \infty$), the expression of the GMR in Eq. (17) is reduced to an effective conductivity spin-asymmetry parameter β_{eff},

$$\beta_{\mathrm{eff}} = \sqrt{\beta^2 - \Delta L^2/\sigma_F^2}. \tag{18}$$

This shows that the GMR is as expected the measure of the spin asymmetry of the conductivity lowered by the spin mixing.

B. MTEP

Now, we apply the model to MTEP measurements. If the matrix $\tilde{Y}$ is derived for a one charge current model, the magnetic information is neglected ($\beta = \Delta L = 0$), and the $\tilde{L}_{\Uparrow,\Downarrow,N}$ matrices are reduced to their top left square submatrices

$$\tilde{L}_F = -\begin{pmatrix} \dfrac{\kappa_F}{T} + \sigma_F \varepsilon_F^2 & \dfrac{\sigma_F \varepsilon_F}{q} \\ \dfrac{\sigma_F \varepsilon_F}{q} & \dfrac{\sigma_F}{q^2} \end{pmatrix}, \tag{19a}$$

$$\tilde{L}_N = -\begin{pmatrix} \dfrac{\kappa_N}{T} + \sigma_N \varepsilon_N^2 & \dfrac{\sigma_N \varepsilon_N}{q} \\ \dfrac{\sigma_N \varepsilon_N}{q} & \dfrac{\sigma_N}{q^2} \end{pmatrix}. \tag{19b}$$

The last term of Eq. (14) accounting for the overall Seebeck coefficient $\bar{\varepsilon}$, then becomes simply

$$\bar{\varepsilon} = \frac{Y_{21}}{q Y_{22}} = \frac{\varepsilon_F \kappa_N + \varepsilon_N \kappa_F}{\kappa_F + \kappa_N}. \tag{20}$$

This is the conventional composition of the Seebeck coefficients in a series circuit.[29,33,34]

C. CPP-Peltier

In order to clarify the concept of the MTGV, it is useful to consider this measurement under the one charge current model. With the matrices in Eqs. (19a) and (19b), we establish the effective resistance of Eq. (14) as

$$\frac{L}{4A}\frac{1}{e^2 Y_{22}} = \frac{L}{2A}\left[\left(\frac{1}{\sigma_F} + \frac{1}{\sigma_N}\right) + T\frac{(\varepsilon_F - \varepsilon_N)^2}{\kappa_F + \kappa_N}\right]. \tag{21}$$

This expression reflects that the current conservation conditions imposed by the 1D structures imply a thermopowerlike term beside the conventional resistance, also proportional to I_{dc}. We call it the CPP-Peltier term since it includes the difference of thermopower across the F/N interface.

The CPP-Peltier term is qualitatively understood as follows: the Peltier effect forces the interfaces to be alternatively heat sources and heat sinks. Therefore a local temperature gradient develops in each layer, alternatively positive and negative. We calculated its magnitude to be

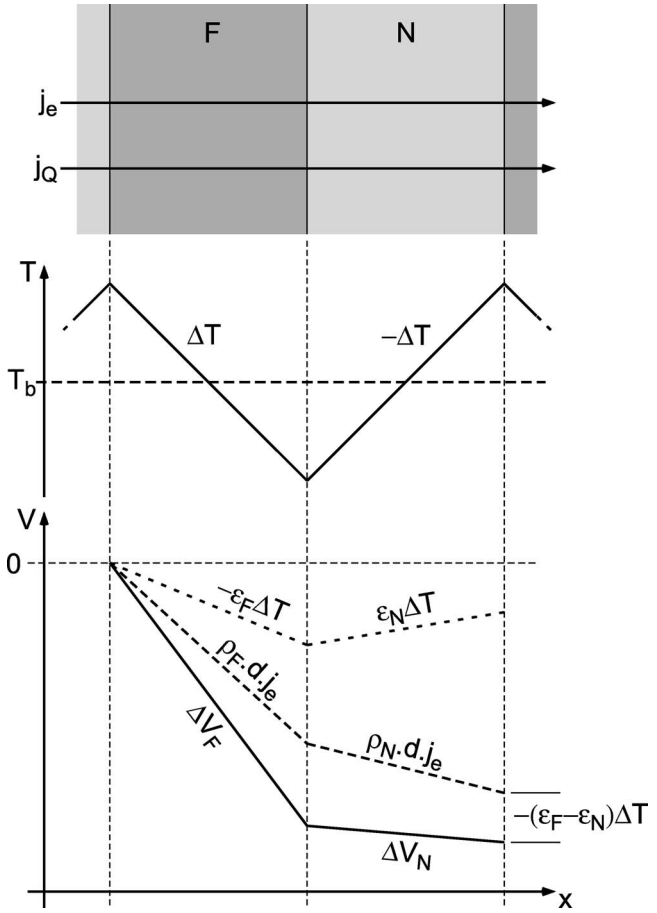

FIG. 6. Up: Co/Cu multilayer structure. The actual aspect ratio (stack height/diameter) of about 1000 insures charge (j_e) and heat (j_Q) currents perpendicular to the layers. Middle: small temperature gradients induced by the Peltier effect. The temperature drop ΔT is given by Eq. (22). Down: overall voltage drop (full line) as the sum of the local Seebeck voltages (dotted line) and Ohm's Law (dashed line).

$$\nabla T_F = \frac{\varepsilon_F - \varepsilon_N}{\kappa_F + \kappa_N} T \frac{I}{A} = -\nabla T_N. \tag{22}$$

It combines the Peltier effect ($(\varepsilon_F - \varepsilon_N)TI$) and the heat conduction in each layer ($\kappa_F + \kappa_N$). This gives the jigsaw temperature profile sketched in Fig. 6. Then the CPP-Peltier voltage is the sum of all the thermoelectrical power induced by the local temperature gradients of each layer.

The magnitude of the CPP-Peltier is so small compared to the resistance that it is negligible in the GMR measurements. Nevertheless, the MTGV measurement protocol takes advantage of an oscillatory heat source. It causes the overall temperature $\bar{T}$ of the wire to oscillate. The ac voltage V_{ac} in phase with the heat source contains a component dependent of the dc current I_{dc}, and derived from the CPP-Peltier term (see Appendix B)

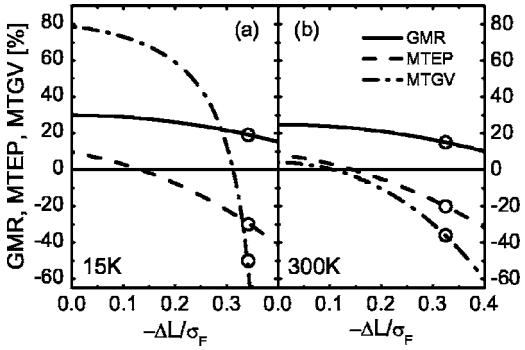

FIG. 7. Calculation of the GMR, MTEP, and MTGV ratios as a function of $-\Delta L/\sigma_F$ (see text) in (a) the low temperature regime and (b) the room temperature regime. The circles recall the experimental values at 15 K (Fig. 3) and 300 K (GMR: 15%; MTEP: −20% and MTGV: −36%).

$$\frac{\partial V_{\rm ac}}{\partial I_{\rm dc}} = \frac{L}{2A} T_{\rm ac} \left[\frac{d}{dT} \left(\frac{1}{\sigma_F} + \frac{1}{\sigma_N} \right) + 2 \frac{(\varepsilon_F - \varepsilon_N)^2}{\kappa_F + \kappa_N} \right]. \quad (23)$$

Under this lock-in measurement, the magnitude of CPP-Peltier term is found comparable to, or larger than, the derivative of the resistance with the temperature. Therefore the MTGV protocole emphasizes the contribution of this CPP-Peltier term.

The dependence of the TGV voltage on the magnetic field is also to be exclusively assigned to the CPP-Peltier term. The argument is twofold: first, the derivative of the resistivity with respect to the temperature is quasi-independent of the magnetic field, and second, in the low temperature range, the resistivity is practically independent of the temperature ($d\rho/dT=0$). Hence, it results that the field dependence of the MTGV is exclusively due to the CPP-Peltier term. That is to say, we measure the magnetic response of the term $(\varepsilon_F - \varepsilon_N)^2$. The three-current model clarifies this magnetic effect.

V. DISCUSSION OF EXPERIMENTS IN TERMS OF THE 3-CURRENT MODEL

A. Spin-mixing effects on GMR, MTEP, and MTGV

We applied the 3-current model to our experimental data collected with the three different experiments. The expressions of GMR, MTEP, and MTGV with the full matrix $\tilde{Y}$ are rather complex algebraic expressions. There is no point in writing them down. Instead we present numerical evaluations using these expressions, for both 300 K and 15 K, i.e., the room temperature regime and the low temperature regime ($d\rho/dT=0$), respectively.

We present now the dependence on the spin-mixing, expressed by the parameter ΔL. It is thought to arise from elastic spin-flip scattering processes induced by electron-magnon collisions.[5,14,35] The spin-mixing parameters L_{+-} and L_{-+} in Eq. (1) are directly proportional to the spin-flip rates τ_{+-}^{-1} and τ_{-+}^{-1}. Their relative amplitudes, estimated as in Ref. 14, are found to follow the relation $L_{-+} > L_{+-}$, that yields $\Delta L < 0$. Therefore we present our calculations in Fig. 7 as a function of the reduced variable $-\Delta L/\sigma_F$.

TABLE I. Numerical values at 15 K used in the calculations presented in Fig. 7.

	15 K	300 K
ρ_F^0 (Ω m)	30×10^{-8}	26.4×10^{-8}
ρ_F' (Ω m/K)	0	2.84×10^{-10}
ρ_N^0 (Ω m)	3×10^{-8}	6.67×10^{-8}
ρ_N' (Ω m/K)	0	6.86×10^{-11}
β^0	0.47	0.454
β'	0	-1.15×10^{-4}
ε_F^0 (μV/K)	−2.7	−2.7
ε_F' (μV/K^2)	−0.1	−0.1
ε_N^0 (μV/K)	0	0
ε_N' (μV/K^2)	−0.084	−0.084

We used in our calculations the numerical values of the transport parameters, determined from our measurements, listed in Table I (Appendix D). The large resistivity of the Co ($\sim 30\times10^{-8}$ Ω m) strongly diminishes the role of interface resistances, not accounted for in our model.

To perform the fitting with the experimental data of GMR, MTEP and MTGV in both temperature regimes (open circles in Fig. 7), we adjusted the values of the parameters β and ε_N, and also of $\alpha_{\rm th}$ that expresses the spin asymmetry of the Seebeck coefficients in absence of spin-mixing [Eq. (A4)],

$$\alpha_{\rm th} = \frac{\varepsilon_\uparrow}{\varepsilon_\downarrow}. \quad (24)$$

β was determined around 0.58 (0.53) at 15 K (300 K). The value of ε_N, reported in Table I (−25.2 μV/K at room temperature) is reasonable for a Cu layer with about 0.5% of Co impurity content.[28,31] Finally a value of 0.7 was determined for $\alpha_{\rm th}$ at all temperatures.

The values of $-\Delta L/\sigma_F$ extracted from the fitting shows little dependence on the temperature, ranging from 0.34 at 15 K to 0.32 at 300 K. This is consistent with mechanisms based on electron-magnon scattering that varies slowly with the temperature.[14]

The GMR prediction in Fig. 7 shows a weak dependence on ΔL only. The calculations with the simpler relation Eq. (17) give the same result as the calculation with the full matrix. This confirms that heat fluxes and the Peltier effect only play a very limited role in the GMR. The fitting values of β are found a bit higher that those reported in other works.[11,31,36] However, the effective conductivity spin asymmetry $\beta_{\rm eff}$, is found to be 0.47 and 0.42 at, respectively, 15 K and 300 K, for the fitting values of $-\Delta L/\sigma_F$. This fits with the values presented in the literature.

The MTEP shows a quasilinear dependence on ΔL. This behavior shows that the more the elastic spin-flip is asymmetric in spin, the more the effective Seebeck coefficients have a spin asymmetry (see Sec. V B). To the contrary, we find that the MTGV is highly sensitive to the change of ΔL, i.e., to the spin asymmetry of the spin-mixing rates. This is especially pronounced at low temperature, for which the resistance contribution to the MTGV vanishes. This shows that

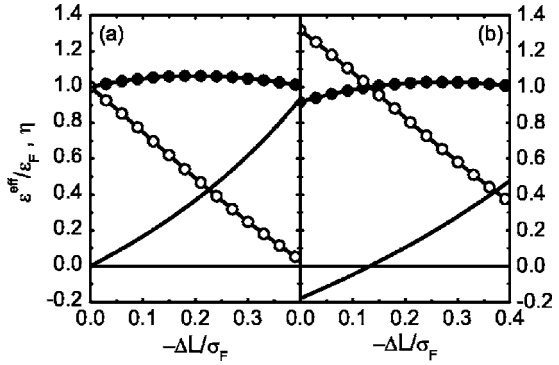

FIG. 8. Effective Seebeck coefficients $\varepsilon_{\uparrow}^{\text{eff}}$ (full circles, ●) and $\varepsilon_{\downarrow}^{\text{eff}}$ (open circles, ○) normalized by ε_F, and the asymmetry parameter η (solid line) as functions of $-\Delta L/\sigma_F$, for (a) $\alpha_{\text{th}}=1$ and (b) $\alpha_{\text{th}}=0.7$.

the MTGV, which arises from the spin-dependent CPP-Peltier effect, provides information that is distinct from the GMR.

B. Effective Seebeck coefficients

In the framework of this three-current model, we can define the effective Seebeck coefficient of each spin channel $\varepsilon_{\uparrow(\downarrow)}^{\text{eff}}=-(1/q)(\nabla\mu_{\uparrow(\downarrow)}+q\nabla V)/\nabla T$ using Eq. (A3) with $j_n=j_p=0$ (Appendix C). Even in the case of equal Seebeck coefficient $\varepsilon_{\uparrow}=\varepsilon_{\downarrow}=\varepsilon_F$ ($\alpha_{\text{th}}=1$), we find a spin asymmetry, $\varepsilon_{\uparrow}^{\text{eff}} \neq \varepsilon_{\downarrow}^{\text{eff}}$, due only to $\Delta L\neq 0$,

$$\varepsilon_{\uparrow}^{\text{eff}} = \varepsilon_F \frac{(1-\beta^2)-(1-\beta)\dfrac{\Delta L}{\sigma_F}}{(1-\beta^2)+\dfrac{\Delta L^2}{\sigma_F^2}}, \tag{25a}$$

$$\varepsilon_{\downarrow}^{\text{eff}} = \varepsilon_F \frac{(1-\beta^2)+(1+\beta)\dfrac{\Delta L}{\sigma_F}}{(1-\beta^2)+\dfrac{\Delta L^2}{\sigma_F^2}}. \tag{25b}$$

It is to be noticed here that the difference between the effective Seebeck coefficients is exclusively induced by the spin-mixing term ΔL. The spin asymmetry η of the Seebeck coefficient, as discussed in Ref. 27, is, according to the three-current model in this case,

$$\eta = \frac{\varepsilon_{\uparrow}^{\text{eff}}-\varepsilon_{\downarrow}^{\text{eff}}}{\varepsilon_{\uparrow}^{\text{eff}}+\varepsilon_{\downarrow}^{\text{eff}}} = \frac{-\dfrac{\Delta L}{\sigma_F}}{1-\beta^2+\beta\dfrac{\Delta L}{\sigma_F}}. \tag{26}$$

From Eqs. (25a), (25b), and (26), we plot the effective Seebeck coefficients and the parameter η in Fig. 8(a) as a function of the dimensionless variable $-\Delta L/\sigma_F$. We set $\beta=0.58$ (low temperature regime).[39] $\varepsilon_{\downarrow}^{\text{eff}}$ is found to decrease strongly, whereas $\varepsilon_{\uparrow}^{\text{eff}}$ remains almost constant, with a spin asymmetry η around 74% for $-\Delta L/\sigma_F=0.34$. The same trend is observed in the plots of Fig. 8(b), performed with $\alpha_{\text{th}}=0.7$, with however a much smaller value of η of 0.35 at the same spin mixing asymmetry.

The existence of the spin asymmetry of the spin-mixing ($\Delta L\neq 0$) is consistent with the quantum-mechanical description of electron-magnon scattering.[14,35]

VI. CONCLUSION

We investigated the mixed effects of heat and charge transport in multilayered magnetic nanostructures with current perpendicular to the interfaces. We introduced a new experiment, which we called magneto-thermogalvanic voltage (MTGV), that detects the voltage drop along a nanowire oscillating at the frequency of the temperature oscillation induced by a chopped heat source. Data are discussed in terms of non-equilibrium thermodynamics in the linear regime. This gives a "three-current model," which joins the entropy current to the two spin charge currents. The magneto-transport matrix elements are derived for both magnetic and nonmagnetic materials, and applied to a layered system with the relevant boundary conditions. We establish then an effective transport matrix for two bilayers in terms of natural transport parameters, from which we can derive simple expressions of the GMR, MTEP, and MTGV. This model predicts that local temperature gradients due to the Peltier effect develop in each layers, and the corresponding local Seebeck voltages add to the overall potential drop. The MTGV measurement emphasizes the contribution of the Peltier effect. Therefore, by its nature, MTGV reveals something different about spin transport than resistivity measurements.

It was shown from numerical estimates using the full 3×3 transport matrix that MTGV is highly dependent on the spin asymmetry of the spin-mixing transition rates ΔL. The same term ΔL contributes to the MTEP and can account for our data without invoking a spin-dependent entropy transport coefficient ($\varepsilon_{\uparrow}=\varepsilon_{\downarrow}$). The model accounts in a consistent manner for the observed values of GMR, MTEP, and MTGV at 15 K and 300 K.

APPENDIX A: DETERMINATION OF THE TRANSPORT MATRIX COEFFICIENTS

The L_{ij} coefficients of Eq. (1) are related to physical parameters according the method of Ref. 29. We apply here this method in the approximation of independent currents, i.e., without spin-mixing ($L_{+-}=L_{-+}=0$).

1. Ohm's Law

Ohm's Law states for each charge current,

$$\sigma = \frac{-qj_n}{\dfrac{1}{q}\nabla\bar{\mu}} \quad \nabla T=0. \tag{A1}$$

Here $\bar{\mu}$ refers to the electrochemical potential, composed of the chemical part μ and the electric part qV, with V the electrostatic potential. For both independent currents + and

−, the gradient is $\nabla\bar{\mu}_{+(-)}=\nabla\mu_{+(-)}-q\mathbf{E}$. Thus we can define the conductivities if the currents are separate,

$$L_{++}=\frac{\sigma_+}{q^2};\quad L_{--}=\frac{\sigma_-}{q^2}. \tag{A2}$$

2. Seebeck coefficient

When there is one type of charge carrier, the Seebeck coefficient is defined by

$$\varepsilon=-\frac{1}{q}\frac{\nabla\bar{\mu}}{\nabla T}\quad j_n=0. \tag{A3}$$

The condition of no charge current ($j_+=j_-=0$) gives for both channels $\nabla\bar{\mu}_\pm=-(L_{s\mp}/L_{\pm\pm})\nabla T$. So it is natural to define

$$\varepsilon_+=\frac{1}{q}\frac{L_{s-}}{L_{++}},\quad \varepsilon_-=\frac{1}{q}\frac{L_{s+}}{L_{--}}. \tag{A4}$$

Combining with Eqs. (A2), we deduce

$$L_{s+}=\frac{\varepsilon_-\sigma_-}{q},\quad L_{s-}=\frac{\varepsilon_+\sigma_+}{q}. \tag{A5}$$

3. Heat conductivity

The conditions are

$$\kappa=\frac{-j_Q}{\nabla T},\quad j_n=0, \tag{A6}$$

with j_Q the heat current that writes from Eq. (1),

$$j_Q=Tj_s=T[-L_{ss}\nabla T-L_{s+}\nabla\bar{\mu}_+-L_{s-}\nabla\bar{\mu}_-]. \tag{A7}$$

The expressions of the electrochemical potential gradients $\nabla\bar{\mu}_+$ and $\nabla\bar{\mu}_-$, derived from the condition of no charge current, are injected in Eq. (A7), giving

$$L_{ss}=\frac{\kappa}{T}+L_{s+}L_{s-}\frac{L_{++}+L_{--}}{L_{++}L_{--}}. \tag{A8}$$

With the expressions of Eqs. (A2)–(A5), we finally establish

$$L_{ss}=\frac{\kappa}{T}+\varepsilon_+\varepsilon_-(\sigma_++\sigma_-). \tag{A9}$$

APPENDIX B: LOCK-IN DETECTION OF THE MTGV IN THE ONE-CURRENT MODEL

Across a nanowire, the voltage drop is proportional to the direct current, as follows from Eq. (21). Applying the Wiedermann-Franz Law ($\kappa=\sigma\mathcal{L}T$, with $\mathcal{L}$ the Lorentz number) to this relation, we find the effective resistance as

$$R_{\text{eff}}=\frac{L}{4A}\frac{1}{e^2Y_{22}}=\frac{L}{2A}\left[\left(\frac{1}{\sigma_F}+\frac{1}{\sigma_N}\right)+\frac{1}{\mathcal{L}}\frac{(\varepsilon_F-\varepsilon_N)^2}{\sigma_F+\sigma_N}\right]. \tag{B1}$$

The MTGV measurement results from the oscillation in temperature of the nanowire. Its amplitude is designated by T_{ac}. The amplitude of the resulting voltage oscillation due to this small temperature oscillation is

$$V_{\text{ac}}=\frac{dR_{\text{eff}}}{dT}I_{\text{dc}}T_{\text{ac}}. \tag{B2}$$

The first derivative of the effective resistance with the temperature writes

$$\frac{2A}{L}\frac{dR_{\text{eff}}}{dT}=\frac{d}{dT}\left(\frac{1}{\sigma_F}+\frac{1}{\sigma_N}\right)+\frac{1}{\mathcal{L}}\frac{(\varepsilon_F-\varepsilon_N)^2}{\sigma_F+\sigma_N}\times\left[2\frac{\frac{d}{dT}(\varepsilon_F-\varepsilon_N)}{\varepsilon_F-\varepsilon_N}-\frac{\frac{d}{dT}(\sigma_F+\sigma_N)}{\sigma_F+\sigma_N}\right]. \tag{B3}$$

In the approximation of Seebeck coefficients linear with the temperature [$\varepsilon=(d\varepsilon/dT)T$], roughly valid for disordered metals, then

$$\frac{\frac{d}{dT}(\varepsilon_F-\varepsilon_N)}{\varepsilon_F-\varepsilon_N}=\frac{1}{T}. \tag{B4}$$

For a metal with a large concentration of impurities, like our samples, $d\sigma/dT\ll\sigma$, then

$$2\frac{\frac{d}{dT}(\varepsilon_F-\varepsilon_N)}{\varepsilon_F-\varepsilon_N}-\frac{\frac{d}{dT}(\sigma_F+\sigma_N)}{\sigma_F+\sigma_N}\simeq\frac{2}{T}. \tag{B5}$$

Then Eq. (B2) is reduced to

$$V_{\text{ac}}=\frac{L}{2A}\left[\frac{d}{dT}\left(\frac{1}{\sigma_F}+\frac{1}{\sigma_N}\right)+\frac{2}{T}\frac{1}{\mathcal{L}}\frac{(\varepsilon_F-\varepsilon_N)^2}{\sigma_F+\sigma_N}\right]I_{\text{dc}}T_{\text{ac}}. \tag{B6}$$

This establishes Eq. (23).

APPENDIX C: CALCULATION OF EFFECTIVE SEEBECK COEFFICIENTS

We defined Seebeck coefficients for separate channels [Eqs. (A3) and (A4)]. Then we define for the two channels the effective Seebeck coefficients as

$$\varepsilon_{\uparrow,\downarrow}^{\text{eff}}=-\frac{1}{q}\frac{\nabla\mu_{\uparrow,\downarrow}+q\nabla V}{\nabla T} \tag{C1}$$

with no charge current, that is, $j_n=j_p=0$. We apply these conditions to the kinetic equations derived from the matrix in Eq. (8).

For the current ↑, we perform the variable changes $\nabla\Delta\mu=\nabla\mu_\uparrow$ and write expressions in terms of $(\nabla\mu_\uparrow+q\nabla V)$. It is then straightforward to establish, from the definition in Eq. (C1),

$$\varepsilon_\uparrow^{\text{eff}}=\frac{(1-\beta)\sigma_F^2\varepsilon_F-\sigma_F\varepsilon_F\Delta L-(1-\beta)\sigma_F\Delta L_S-\Delta L\Delta L_S}{(1-\beta^2)\sigma_F^2+\Delta L^2}. \tag{C2}$$

We apply the same calculation for the channel ↓, with $\nabla\Delta\mu=-\nabla\mu_\downarrow$, letting the term $(\nabla\mu_\downarrow+q\nabla V)$ appear. It yields

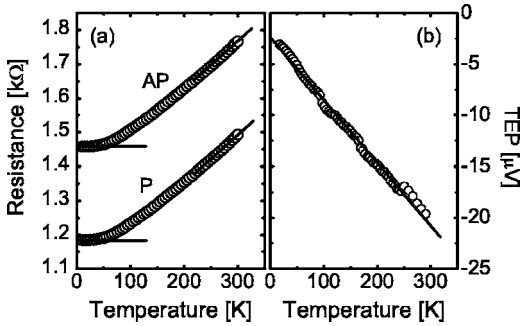

FIG. 9. Typical temperature dependence of transport measurements on Co/Cu multilayer nanowires. (a) Resistances for the both parallel (P) and antiparallel (AP) configurations. The solid lines model the temperature dependence for the low and room temperature regimes. (b) TEP at zero field. The solid line fits the linear dependence on the temperature over all the temperature range.

$$\varepsilon_{\downarrow}^{\text{eff}} = \frac{(1+\beta)\sigma_F^2\varepsilon_F + \sigma_F\varepsilon_F\Delta L + (1+\beta)\sigma_F\Delta L_S - \Delta L\Delta L_S}{(1-\beta^2)\sigma_F^2 + \Delta L^2}. \tag{C3}$$

The coefficient ΔL_S is related to the natural spin asymmetry of the Seebeck coefficients $\alpha_{\text{th}}=\varepsilon_{\uparrow}/\varepsilon_{\downarrow}$ via the relation

$$\Delta L_S = \sigma_F\varepsilon_F\frac{1-\beta-\alpha_{\text{th}}(1+\beta)}{1-\beta+\alpha_{\text{th}}(1+\beta)}. \tag{C4}$$

Under the condition $\alpha_{\text{th}}=1$, i.e., $\varepsilon_{\uparrow}=\varepsilon_{\downarrow}=\varepsilon_F$, that induces $\Delta L_S=-\beta\sigma_F\varepsilon_F$, we get the simpler expressions in Eqs. (25a) and (25b).

APPENDIX D: PARAMETERS NUMERICAL VALUES FOR NUMERICAL CALCULATIONS

Our numerical calculations were performed with the parameters presented in Table I. The resistivities and Seebeck coefficients were determined from the temperature dependence of the measured resistance and thermoelectrical power (Fig. 9). The other parameters were deduced by fitting consistently at 15 K and 300 K all three measurements: GMR, MTEP, and MTGV.

Under the conditions expressed in Sec. IV A (constant temperature), we easily establish the expressions of the resistance in the parallel (P) and in the antiparallel (AP) magnetic configurations, as

$$R_P = \frac{L}{\pi r_0^2}\frac{\rho_F^2 + 2\rho_F\rho_N + \rho_N^2(1-\beta^2)}{\rho_F + \rho_N(1-\beta^2)}, \tag{D1}$$

$$R_{\text{AP}} = \frac{L}{\pi r_0^2}\frac{\rho_F + \rho_N(1-\beta^2)}{1-\beta^2}. \tag{D2}$$

The subsequent GMR is expressed in Eq. (15). Here the resistivities are expressed as

$$\rho_{F,N}(T) = \rho_{F,N}^0 + \rho'_{F,N}T \tag{D3}$$

with the intercept ρ^0 as a free parameter, and $\rho'=d\rho/dT$ taken from the tables for pure Co and Cu in Ref. 37. In a similar way, we also define

$$\beta_{\text{eff}}(T) = \beta_{\text{eff}}^0 + \beta'_{\text{eff}}T. \tag{D4}$$

The fitting with the data in Fig. 9(a) for both temperature regimes yields the experimental values listed in Table I. They are consistent with previous works on similar structures.[31] A wire diameter r_0 of 21 nm is found, which is consistent with the specifications of the template.

Following the Matthiesen's rule, we considered two different temperature regimes: (i) the low temperature regime, for which resistivity of metals are independent of the temperature, and (ii) the room temperature regime, for which resistivities are linear with the temperature.

The thermoelectrical power measured at zero magnetic field is found to be linear with the temperature, as expected for metals.[28] The rather high impurity density prevents any deviation from phonon-drag processes. Applying the Wiedermann-Franz Law to Eq. (20), the composition of the Seebeck coefficients in series circuit is

$$\bar{\varepsilon} = \frac{\varepsilon_F\rho_F + \varepsilon_N\rho_N}{\rho_F + \rho_F}. \tag{D5}$$

Here also we set a linear temperature dependence of the Seebeck coefficients over the whole range of temperatures,

$$\varepsilon_{F,N}(T) = \varepsilon_{F,N}^0 + \varepsilon'_{F,N}T. \tag{D6}$$

With the value of resistivities in Table I, we adjusted the parameters $\varepsilon_{F,N}$ to fit Eq. (D5) with the data in Fig. 9(b). However, the predominance of ρ_F over ρ_N allows ε_F only to be directly determined. The fitting procedure in Sec. V A gave the values of ε_N.

*Electronic address: Laurent.Gravier@epfl.ch

[1] F. Lowance and F. Woodbridge Constant, Phys. Rev. **48**, 257 (1935).
[2] J. -P. Jan, *Solid State Physics* (Academic, New York, NY, 1957), Vol. 5.
[3] M. Baylin, Phys. Rev. **126**, 2040 (1962).
[4] A. Fert and I. A. Campbell, Phys. Rev. Lett. **21**, 1190 (1968).
[5] G. N. Grannemann and L. Berger, Phys. Rev. B **13**, 2072 (1976).
[6] G. Herzer, J. Magn. Magn. Mater. **45**, 345 (1984).
[7] P. Grunberg, R. Schreiber, Y. Pang, M. B. Brodsky, and H. Sowers, Phys. Rev. Lett. **57**, 2442 (1986).
[8] M. N. Baibich, J. M. Broto, A. Fert, F. Nguyen Van Dau, F. Petroff, P. Etienne, G. Creuzet, A. Friederich, and J. Chazelas, Phys. Rev. Lett. **61**, 2472 (1988).
[9] W. P. Pratt, S. -F. Lee, J. M. Slaughter, R. Loloee, P. A. Schroeder, and J. Bass, Phys. Rev. Lett. **66**, 3060 (1991).

[10] M. A. M. Gijs, S. K. J. Lenczowski, and J. B. Giesbers, Phys. Rev. Lett. **70**, 3343 (1993).
[11] T. Valet and A. Fert, Phys. Rev. B **48**, 7099 (1993).
[12] J. Sakurai, M. Horie, S. Araki, H. Yamamoto, and T. Shinjo, J. Phys. Soc. Jpn. **60**, 2522 (1991).
[13] M. J. Conover, M. B. Brodsky, J. E. Mattson, C. H. Sowers, and S. D. Bader, J. Magn. Magn. Mater. **102**, L5 (1991).
[14] L. Piraux, A. Fert, P. A. Schroeder, R. Loloee, and P. Etienne, J. Magn. Magn. Mater. **110**, L247 (1992).
[15] J. Shi, K. Pettit, E. Kita, S. S. P. Parkin, R. Nakatani, and M. B. Salamon, Phys. Rev. B **54**, 15273 (1996).
[16] S. Baily, M. B. Salamon, and W. Oepts, J. Appl. Phys. **87**, 4855 (2000).
[17] M. Johnson and R. H. Silsbee, Phys. Rev. B **35**, 4959 (1987).
[18] M. Johnson, J. Supercond. **16**, 679 (2003).
[19] J. -E. Wegrowe, Phys. Rev. B **62**, 1067 (2000).
[20] L. Gravier, S. Serrano-Guisan, and J. -P. Ansermet, J. Appl. Phys. **97**, 10C501 (2005).
[21] A. Blondel, J. -P. Meier, B. Doudin, and J. -P. Ansermet, Appl. Phys. Lett. **65**, 3020 (1994).
[22] L. Piraux, J. George, J. Despres, C. Leroy, E. Ferain, R. Legras, K. Ounadjela, and A. Fert, Appl. Phys. Lett. **65**, 2484 (1994).
[23] T. Ohgai, X. Hoffer, A. Fábián, L. Gravier, J. -E. Wegrowe, and J.-P. Ansermet, J. Mater. Chem. **13**, 2530 (2003).
[24] J. -E. Wegrowe, S. E. Gilbert, D. Kelly, B. Doudin, and J. -P. Ansermet, IEEE Trans. Magn. **34**, 903 (1998).
[25] P. Guittienne, L. Gravier, J. -E. Wegrowe, and J. -P. Ansermet, J. Appl. Phys. **92**, 2743 (2002).
[26] L. Gravier, A. Fábián, A. Rudolf, A. Cachin, K. Hjort, and J. -P. Ansermet, Meas. Sci. Technol. **15**, 420 (2004).
[27] L. Gravier, A. Fábián, A. Rudolf, A. Cachin, J. -E. Wegrowe, and J. -P. Ansermet, J. Magn. Magn. Mater. **271**, 153 (2004).
[28] J. Bass, J. Dugdale, C. Foiles, and A. Myers, *Landolt-Boernstein, Numerical Data and Functional Relationships in Science and Technology, Group III* (Springer-Verlag, Berlin, 1985), Vol. 15b.
[29] H. B. Callen, *Thermodynamics* (Wiley, New York, 1960).
[30] P. Atkins and J. de Paula, *Atkin's Physical Chemistry* (Oxford University Press, Oxford, 2002).
[31] B. Doudin, A. Blondel, and J. -P. Ansermet, J. Appl. Phys. **79**, 6090 (1996).
[32] J. -P. Ansermet, J. Phys.: Condens. Matter **10**, 6027 (1998).
[33] J. S. Dugdale, *The Thermoelectrical Properties of Metals and Alloys* (Edward Arnold, London, 1977).
[34] R. D. Barnard, *Thermoelectricity in Metal and Alloys* (Taylor and Francis, London, 1972), p. 143.
[35] I. Y. Korenblit and Y. P. Lazarenko, Sov. Phys. JETP **33**, 837 (1971).
[36] M. A. M. Gijs, A. Reinders, R. M. Jungblut, W. Oepts, and W. J. W. de Jonge, J. Magn. Magn. Mater. **165**, 17 (1997).
[37] J. Bass and K. H. Fischer, *Landolt-Boernstein, Numerical Data and Functional Relationships in Science and Technology, Group III* (Springer-Verlag, Berlin, 1982), Vol. 15a.
[38] Equation (17) can be also deduced from Eqs. (44)–(45) of Ref. 11 for $\Delta L=0$, by neglecting the interface resistances.
[39] The same plot at room temperature is almost identical.